ELSEVIER

Journal of Non-Crystalline Solids 290 (2001) 153–162

JOURNAL OF NON-CRYSTALLINE SOLIDS

www.elsevier.com/locate/jnoncrysol

Organic–inorganic hybrid coatings for corrosion protection

T.P. Chou [a], C. Chandrasekaran [b], S.J. Limmer [a], S. Seraji [a], Y. Wu [a], M.J. Forbess [a], C. Nguyen [a], G.Z. Cao [a,*]

[a] *Department of Materials Science and Engineering, University of Washington, Roberts Hall 302M, Box 352120, Seattle, WA 98195-2120, USA*

[b] *Boston Scientific Corporation, Redmond WA, USA*

Received 25 April 2001

Abstract

The corrosion resistance of sol–gel derived, organic–inorganic, silica-based hybrid coatings with various amounts of organic content was studied. Hybrid sols were prepared by copolymerizing tetraethylorthosilicate (TEOS) and 3-methacryloxypropyltrimethoxysilane (MPS) with a two-step acid-catalyst process. Hybrid coatings were dip-coated on 304 stainless steel substrates and annealed at 300 °C for 30 min. Such prepared hybrid coatings were found to be relatively dense, uniform and defect free. The adhesion and flexibility of the coatings were characterized. The influences of the amount of organic component incorporated into the coatings and the aging of sols on corrosion protection were studied. Electrochemical analyses showed that the relatively dense hybrid coatings provided excellent corrosion protection by forming a physical barrier, which effectively separated the anode from the cathode. Some preliminary biocompatibility tests were also conducted on the hybrid coatings. © 2001 Elsevier Science B.V. All rights reserved.

1. Introduction

Corrosion is a loss of material due to the electrochemical interaction with the environment and the electrochemical reactions involving electron transfer; therefore, one of the most effective corrosion control techniques is to electrically isolate the anode from the cathode [1,2]. For example, the chromium oxide (Cr_2O_3) passivation layer formed on the surface of stainless steel in oxidizing environments is the main reason for its corrosion resistance and durability [2,3]. A more generic approach to enhance corrosion resistance is to apply protective films or coatings such as paint. Such protective coatings also permit the introduction of other desired chemical and physical properties, such as mechanical strength, hydrophobicity, and biocompatibility, through the modification of chemical composition of the coatings. Various organic coatings have been studied for corrosion protection [4–6]. Densely packed, self-assembled monolayers of alkanethiol on an oxide-free surface of copper were also reported to be effective for blocking certain electrochemical processes, thus, making them candidates for corrosion protection of copper metallization in electronic devices [7,8]. Various oxide coatings by sol–gel processing have been studied extensively for corrosion protection of stainless steel [9–13]. In spite of all the advantages of sol–gel processing, sol–gel oxide coatings suffer from several drawbacks. In general, sol–gel coatings are highly

* Corresponding author.
E-mail address: gzcao@u.washington.edu (G.Z. Cao).

0022-3093/01/$ - see front matter © 2001 Elsevier Science B.V. All rights reserved.
PII: S0022-3093(01)00818-3

porous with low mechanical integrity; annealing or sintering at high temperatures (>800 °C) is required to achieve a dense microstructure [14–17]. Sintering at high temperatures might introduce cracks and/or delamination of sol–gel coatings due to a large mismatch of thermal expansion coefficients and possible chemical reactions at the interface. Sintering at high temperatures also limits application of sol–gel coatings on temperature sensitive substrates and devices. Furthermore, high temperature sintering prevents the incorporation of functional organic and bio-components into sol–gel oxide coatings, which greatly limits the applications of sol–gel-derived oxide coatings. It is obviously very important to develop dense sol–gel-derived hybrid coatings without post-deposition sintering or annealing at elevated temperatures.

One viable approach to dense, sol–gel-derived coatings without post-deposition annealing at elevated temperatures is to synthesize organic–inorganic hybrid coatings. When appropriate chemical composition and processing conditions were applied, relatively dense organic–inorganic hybrid coatings were developed for applications including wear resistance [18,19] and corrosion protection [20–22]. Messaddeq et al. [21] studied corrosion resistance of organic–inorganic hybrid coatings on stainless steel. The coatings were made by dispersing various amounts of polymethylmethacrylate (PMMA) into zirconia (ZrO_2) sol and fired at 200 °C for 30 min. PMMA-ZrO_2 coatings demonstrated promising corrosion resistance and increased the lifetime of the stainless steel by a factor 30 [21]. However, phase segregation, incomplete coverage, and delamination were observed when the coatings consisted of a high content of organic components. In this paper, we studied the corrosion resistance of sol–gel-derived, organic–inorganic hybrid coatings on stainless steel. The current research was also aimed at developing corrosion protecting, sol–gel coatings with desired flexibility and biocompatibility. Sol–gel-derived coatings were made from tetraethylorthosilicate (TEOS) and 3-methacryloxypropyltrimethoxysilane (MPS) using a two-step acid catalysis process, and were annealed at 300 °C for 30 min. It was demonstrated that sol–gel derived hybrid coatings could significantly enhance the corrosion protection of stainless steel substrates. The relationships between the amount of organic components, processing conditions, and corrosion protection were studied. Corrosion resistance of multiple coatings and adhesion were also discussed. Efforts were also made to understand the possible failure mechanism of corrosion protection by hybrid coatings.

2. Experimental

2.1. Sol preparation

Various compositions of silica-based organic–inorganic hybrid sols were prepared with an acid-catalyzed, two-step hydrolysis–condensation process. Amounts of organic and inorganic components were utilized to control the flexibility and density of the sol–gel network. The hybrid sol was prepared by admixing a silica precursor, tetraethylorthosilicate ($TEOS, Si(OC_2H_5)_4$), and an organic component, 3-methacryloxypropyltrimethoxysilane ($MPS, H_2CC(CH_3)CO_2(CH_2)_3Si(OCH_3)_3$). To prevent any evaporation of chemicals at an elevated temperature, a sealed reaction kettle consisting of a water condenser attachment, a magnetic stir bar, and a thermocouple was used.

Three compositions of the sol were prepared for analysis; silica (SiO_2) sols containing 5, 10, and 20 mol% MPS each had a TEOS:MPS ratio of 95:5, 90:10, and 80:20, respectively. An initial stock solution was made for each composition by dissolving specific amounts of TEOS and MPS in a mixture of ethanol (C_2H_5OH), deionized water (DI H_2O), and 1 N hydrochloric acid (HCl), which acts as the catalyst in the reaction. Each stock solution contained a TEOS:MPS:C_2H_5OH:DI H_2O:HCl nominal molar ratio of 0.95:0.05:3.8:5:4.8×10^{-3}, 0.90:0.10:3.8:5: 4.8×10^{-3}, and 0.80:0.20:3.8:5:4.8×10^{-3} for SiO_2 sols containing 5%, 10%, and 20% MPS, respectively. Each combined mixture was vigorously stirred at a rate of 500 rpm for 90 min at a temperature of 60 °C to obtain a stable sol. Further processing of the sol required an additional 3.6 ml 1 N HCl and 1.2 ml DI H_2O to 30 ml of the stock solution. The sol was

then vigorously stirred again at a rate of 500 rpm for 60 min at a temperature of 60 °C. Prior to dip-coating, ethanol was added to dilute the sol in order to obtain a volume ratio of 2:1 ethanol to solution. The mixture was stirred for 1 min and unused portions were stored at freezing temperature (−20 °C) to stabilize the reaction; undiluted sols were also stored at −20 °C.

2.2. Substrate preparation

The substrates (10 mm × 40 mm in dimension) used for the analysis of the sol–gel coatings were 304 stainless steel that had been electro-polished or exposed to nitric acid (HNO_3) to decrease the iron content and increase the chromium content at the surface. Silicon wafers were also used for reference samples. In order to ensure a tight bond and good adhesion between the substrate surface and the sol–gel coating, the substrates were exposed to surface etching at an elevated temperature so as to introduce hydroxyl groups onto the surface of the substrate. Each substrate was initially rinsed with DI H_2O, cleaned with ethanol to remove excess dirt and grease, and air-dried. The preparation of the etching solution consisted of reacting 30% hydrogen peroxide (H_2O_2) with concentrated sulfuric acid (H_2SO_4). The etching solution contained a 30:70 volume ratio of H_2O_2:H_2SO_4, and was initially heated to a temperature of 90 °C [23]. The substrates were then immersed into the etching solution for approximately 30 min. A DI H_2O rinse was used to wash excess etchant remaining on the surface after removing the substrate from the etching solution. Unused, etched substrates were then stored in DI H_2O solution. Etched substrates exposed to air for more than 48 h required re-etching.

2.3. Film deposition

The three prepared sol solutions with varying compositions were used to deposit the sol onto the substrates by way of a dip-coating process. The solutions were initially dispersed and brought back up to room temperature through a 5 min ultrasonication process. Each substrate was dipped into the sol at a constant speed of 140 mm/min using a dip-coater, immersed into the sol for 1 min, and then withdrawn at approximately the same constant speed previously mentioned. The coating was air-dried onto the substrate surface and placed in a furnace to initiate post-deposition heat treatment. The coated substrates were heated at a low temperature of 300 °C for approximately 30 min at a heating and cooling rate of 5 °C/min. Additional sol–gel layering of the substrate required the repetition of the above-mentioned dip-coating procedure.

2.4. Electrochemical analyses

All measurements were performed under extreme environmental conditions consisting of an aqueous, air-exposed, saturated sodium chloride (32% NaCl) solution. Each sample was sealed with waterproof tape in order to prevent premature corrosion along the edges of the substrate. A 7.0 mm × 10 mm area within the center of each sample was exposed to the solution during testing. For flexed samples, the Instron 4505™ machine was used to provide a consistent and reliable flexural procedure to accommodate a specific degree of bending along the substrate to test the coating flexibility by way of corrosion analysis. The substrate was supported at each end and a metal bar with a ~6.0 mm diameter was pressed down horizontally onto the center of the substrate until a displacement of 10 mm was obtained.

Corrosion analysis of bare and coated substrates was done using a potentiostat connected to a corrosion analysis software program. Polarization measurements were carried out potentiostatically at room temperature using a saturated calomel reference electrode (SCE) and a platinum counter electrode. The potentiodynamic measurements were taken within the range of −1000 to 1200 mV versus SCE at a rate of 2 mV/s. Chloride ions within the salt solution cause much of the 'noise' present in the polarization curves; therefore, potentiodynamic data measurements obtained were approximated. Prior to the measurements, each sample was immersed in 32% NaCl solution for at least 15 min.

2.5. Characterization

Optical microscopy, atomic force microscopy (AFM), and scanning electron microscopy (SEM) were also performed on the bare and coated substrates to characterize the surface morphology. Using these methods, the bare and coated substrates before and after running the corrosion test were compared. Ellipsometry and tape tests were also done to indicate the coating thickness and the adhesion of the sol–gel coating to the substrate surface, respectively.

2.6. Biocompatibility test

The organic–inorganic hybrid coatings were also characterized by means of cytoxicity and hemolysis. The test device was extracted in minimal essential media (MEM) for 24 h at 37 °C . The extract was plated in triplicate onto mouse heteroploid connective tissue cells (L-929) and incubated for 48 h at 37 °C. Each plate was then examined microscopically and scored for the degree of morphological cytotoxicity. For the hemolysis analysis, the test device was extracted in 0.9% normal saline for xx hours at xx °C at a ratio of 4 g per 20 ml. The extract was placed in direct contact with fresh, human whole blood. The blood was exposed to the sample for 1 h at 37 °C. Following the exposure, the samples were centrifuged and the optical density of the fluid was read using a spectrophotometer.

3. Results and discussion

Both optical microscopy and SEM observations revealed that uniform, homogeneous, and crack-free hybrid sol–gel coatings on stainless steel substrates were readily obtained prior to and after post-deposition annealing at 300 °C for 30 min. No heat treatment at temperatures above 300 °C was attempted for two reasons. One is to preserve the organic component that was introduced into the system to make the coatings flexible. The organic component, or the methacryloxypropyl group, would pyrolyze at approximately 350 °C [24]. If the organic component is pyrolyzed, the sol–gel coatings would be porous and densification at high temperatures would be required. Another reason is to avoid the formation of cracks in sol–gel coatings, which may result from different thermal expansion coefficients of silica and stainless steel substrates. It was found that the organic component was homogeneously dispersed in the silica gel network and no phase segregation was detectable, which agrees very well with the literature [18,24]. Fig. 1 shows the typical AFM image of hybrid coatings on a stainless steel substrate, and indicates that sol–gel coatings have a smooth surface morphology, regardless of the amount of organic component incorporated into the silica gel network. Ellipsometry analyses revealed that the thickness of the coatings on silicon wafers increased with the amount of organic components, whereas, the refractive indices remained almost the same. The refractive indices and the thickness of the coatings, together with the gelation time of the sols with various amounts of organic components, are summarized in Table 1. The increase in thickness of the coatings with a large fraction of organic component could be explained by the increase in viscosity. The relatively constant refractive indices could be ascribed as a combination of a relatively lower refractive index of the organic component and an increased relative density with an increasing amount of organic component in the SiO_2-MPS system. Incorporation of organic components would lead to reduced connectivity of the silica gel network and reduced condensation reaction rates (i.e., a longer gelation time), which in turn, would result in a denser microstructure of gel network upon the removal of solvent.

Fig. 2 shows the typical polarization curves of both bare and 10% MPS sol–gel coated stainless steel substrates. The polarization curve of the sol–gel coating was appreciably different from that of the bare stainless steel substrate. First, the open circuit potential, E_{oc}, of the sol–gel coatings was significantly lower than that of the bare stainless steel substrate. A reduced open circuit potential might be due to the effective suppression of the cathodic reaction (SiO_2 has a low isoelectric point, leading to a negative surface charge at $pH > 2$). Secondly, a passivation region with a rather low passivation current density of

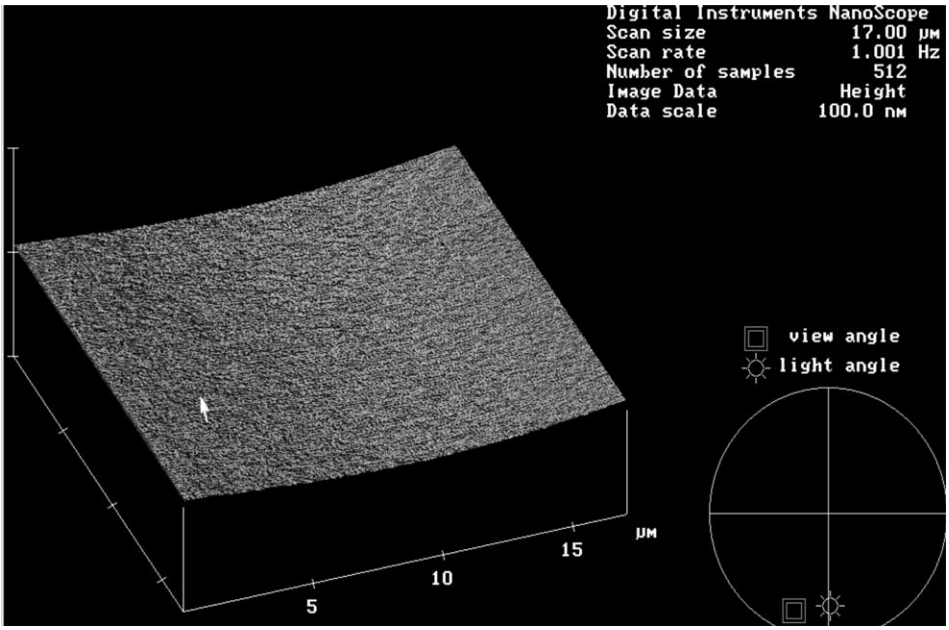

Fig. 1. AFM image of 10% MPS sol–gel coating on a stainless steel substrate.

Table 1
Gelation time, refractive indices and coating thickness of sol–gel coatings incorporated with various amounts of MPS[a]

Coatings	Gelation time (h)	Refractive index	Coating thickness (nm)
5% MPS	88	1.420 ± 0.002	188 ± 2
10% MPS	350	1.415 ± 0.002	201 ± 1
20% MPS	>500	1.417 ± 0.001	235 ± 3

[a] Both refractive indices and coating thickness of sol–gel coatings on silicon wafers were determined by means of ellipsometry.

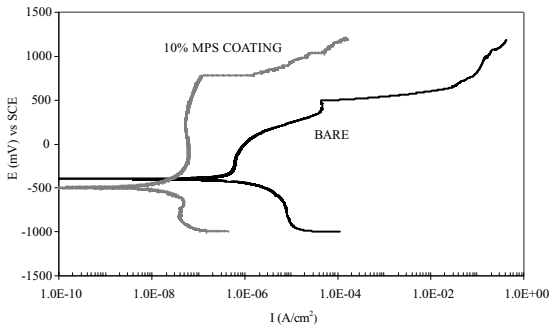

Fig. 2. Polarization curves of bare and 10% MPS sol–gel coated stainless steel substrates.

$\sim 3.5 \times 10^{-8}$ A/cm^2, was present, which implied that the sol–gel coatings indeed provided a physical barrier for blocking the electrochemical process. Such a barrier would fail only at a high electric potential of ~770 mV. The bare stainless steel substrate exhibited a significantly different potentiostat polarization curve and no obvious passivation region was found. As the electric field increased above its E_{oc}, the current density initially increased rapidly, indicating an active electrochemical reaction. The increase of current density slowed down at a current density of $\sim 10^{-7}$ A/cm^2, indicating the possible formation of a passivation layer. Further increase in electric potential resulted in a rapid increase in the current density. This is the typical polarization curve of stainless steel [1]. Thirdly, the open circuit current density of the sol–gel coatings was far smaller than that of the bare stainless steel substrate. The protection efficiency, P, of the sol–gel

coatings on the stainless steel substrates could be calculated by [25]

$$P(\%) = 100(1 - i_{cor}/i^0_{cor}),$$

where i^0_{cor} and i_{cor} denote corrosion current densities of the bare and coated electrodes, respectively. The corrosion current density was obtained from the intersection of the anodic and cathodic Tafel lines. The corrosion protection efficiency of the sol–gel-derived 10% MPS coating was found to be ~98%. Similar corrosion protection efficiency was found in the sol–gel coatings with 5% and 20% MPS studied in this research.

The corrosion protection properties of sol–gel derived coatings are strongly dependent on the processing conditions. In this research, a two-step acid catalyst process was applied in the sol preparation. With this approach, linear silica polymer chains were formed. When dip-coated on a substrate, a sol–gel network based on such linear silica chains would undergo an extensive collapse leading to the formation of dense film upon removal of solvent during drying [26]. However, aging would result in further condensation reaction and consequently the formation of a stronger network, which would resist the capillary force and prevent the formation of a dense sol–gel coating. Aging was found to have a significant influence on the corrosion protection of the sol–gel coatings. For example, the coatings from fresh sols showed enhanced corrosion resistance as compared to that from the aged sols. Fig. 3 shows the polarization curves of 10% MPS coatings, of which one was freshly prepared and another aged for 15 days at room temperature. The sample with the fresh sol showed a much better passivation behavior than the substrate with the aged sol. The potential of the passive region, ΔE_p, defined as the difference between the breakdown and the primary passivation potential, decreased from approximately 1130 to 520 mV for the substrates coated with the fresh and aged 10% MPS sols, respectively, and the breakdown potential decreased from 770 to 115 mV. In addition, the passivation current density was significantly increased from approximately 0.03 to 0.75 $\mu A/cm^2$ for the fresh sol coating to the aged sol coating, a reduction factor of ~20. The differences in the breakdown potential, passivation region and passivation current density indicated that a coating from aged sols is less effective in corrosion protection than a coating from fresh sols. One possible explanation is that the coatings made from a fresh sol had low porosity and/or a larger thickness than those of the coatings from an aged sol. Thicker coatings made from fresh sol is not likely, since the viscosity of a sol increases with the aging time due to the continued condensation reaction. Aging led to an extended condensation reaction, which resulted in the growth of larger silica polymers and the formation of a stronger gel network. Upon removal of solvent during drying, aged sols with larger polymers and a stronger gel network would be more resistant to the capillary-driven collapse of the gel network, resulting in the formation of a more porous structure.

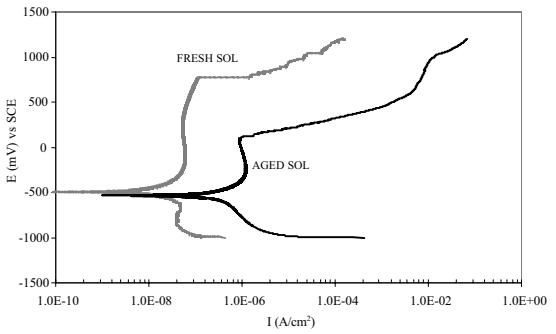

Fig. 3. Polarization curves of stainless steel substrates coated with fresh and aged 10% MPS sols.

Although all three compositions, namely 5%, 10% and 20% MPS, studied in this research showed similar corrosion protection, 5% MPS sol–gel coating did not possess the excellent flexibility that both 10% and 20% MPS hybrid coatings demonstrated. Fig. 4 compares the polarization curves of 10% MPS coatings from aged sol on stainless steel substrates. Two samples were prepared in the same manner, except one was subjected to flexure prior to the polarization test. Fig. 4 clearly shows that the two polarization curves are identical, indicating that the flex test had introduced no detectable influence on the hybrid coatings. This implies that there were neither cracking in the coating nor delamination at the

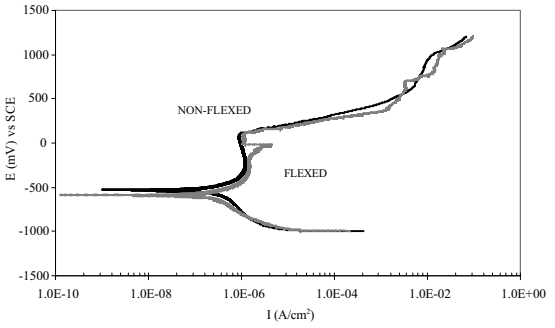

Fig. 4. Polarization curves of non-flexed and flexed stainless steel substrates with 10% MPS sol–gel coatings.

interface. Such an excellent flexibility of sol–gel derived hybrid coatings could be attributed to the incorporation of organic components. However, 5% MPS coatings did not possess the desired flexibility as demonstrated by both 10% and 20% MPS hybrid coatings, due to the relatively reduced amount of organic component incorporated into the system.

Fig. 5 compares the polarization curves of 1-layer and 2-layer coatings on stainless steel using an aged 10% MPS sol–gel composition. The open circuit potential, open circuit current density, passivation potential, and passivation current density were different between the 1-layer and 2-layer coated samples. The two-layer coating demonstrated appreciably enhanced corrosion protection. The 2-layer coating is anticipated to have double the thickness as compared to the 1-layer coating. Diffusion rate or conduction current density through a thicker coating would be less

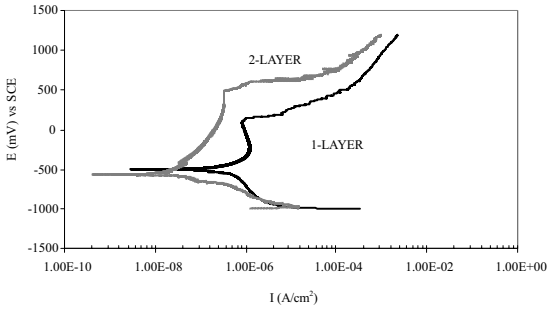

Fig. 5. Polarization curves of stainless steel substrates with 1-layer and 2-layer 10% MPS sol–gel coatings.

than that through a thin coating provided that both coatings have the same physical and chemical properties. An additional layer of 10% MPS sol–gel increased the breakdown potential from approximately 140 to approximately 590 mV, and the potential in the passive region doubled from approximately 620 to approximately 1180 mV. The doubled potential of the passive region could be ascribed to the doubled thickness from the two-layer hybrid coating. Increased coating thickness would withstand higher electric potential if dielectric breakdown is the failure mechanism. Increased coating thickness would also be more resistive to induced interface corrosion failure. Possible failure mechanisms are to be discussed next. This shows that a multi-layer system of coatings does improve the corrosion-resistance of the stainless steel substrates even further by increasing the hindrance of the ability of 'active' chloride ions to flow from the solution to the metal surface.

Fig. 6 compares the SEM images of the bare and 10% MPS sol–gel coated stainless steel substrates after potentiostat polarization tests. Although significant corrosion was found in both samples, the extent of corrosion was appreciably different. The corrosion pits in the bare substrate are much larger than that in sol–gel coated substrates. In addition, the number of pits in the bare substrate was more than that in the coated substrate. The corrosion pits in the sol–gel-coated samples are believed to have formed after the electric potential exceeded the breakdown potential. Fig. 2 showed that the hybrid coating provided a barrier, which resulted in the passivation region. This barrier broke down at high electric potential and resulted in a failure of corrosion protection. There are two possible mechanisms. One is that the hybrid coatings had a dielectric breakdown as the electric potential exceeded its dielectric strength. Another possible mechanism is the interface corrosion. Although the hybrid coatings are relatively dense, there are microscopic pores as evidenced by carbon dioxide sorption isotherms reported by Lu et al. [27]. Some corrosive ions such as chlorine anions might diffuse through these microscopic pores and react with iron at the interface between the hybrid coating

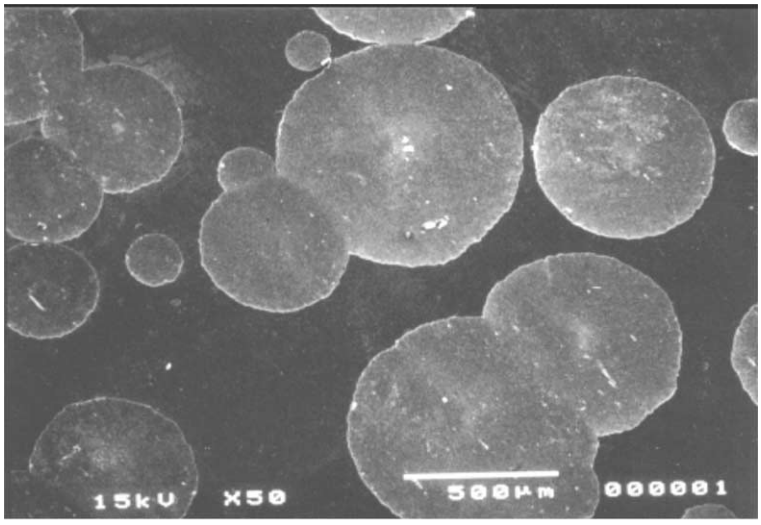

(a)

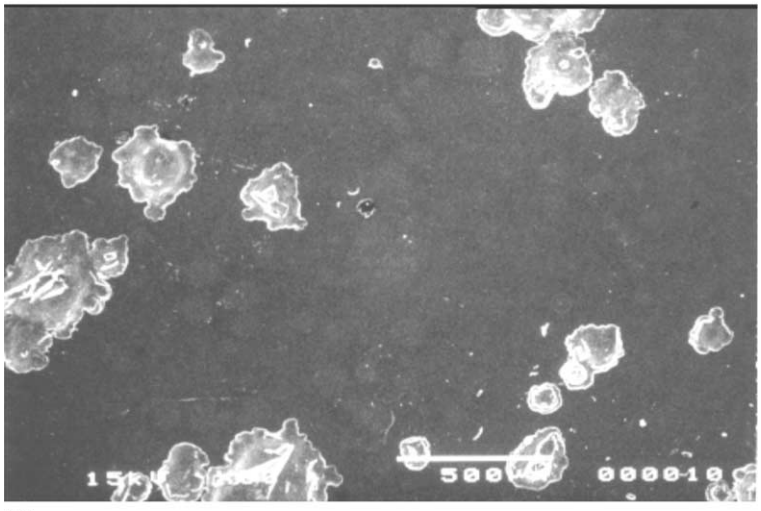

(b)

Fig. 6. SEM images of: (a) bare and (b) 10% MPS sol–gel coated stainless steel substrates after corrosion pitting from polarization analysis.

and substrate. This corrosion process would continue at the interface and result in debonding, delamination, and lifting of sol–gel coatings from the substrate due to a volume expansion as a result of metal oxidation.

Fig. 7(a) is another SEM image of a corrosion pit on a sol–gel coated substrate, the same sample as that shown in Fig. 6(b) at a higher magnification. Fig. 7(a) shows that the hybrid coating was indeed debonded and lifted from the substrate, and thus suggests that interface corrosion is more likely the mechanism, which resulted in the breakdown. Fig. 7(b) is a simplified schematic drawing to illustrate the debonding, delamination and lifting of the sol–gel coatings from the substrates. Debonding between the sol–gel coating and the substrate could be attributed at least partly to hydrolysis reactions at the interface,

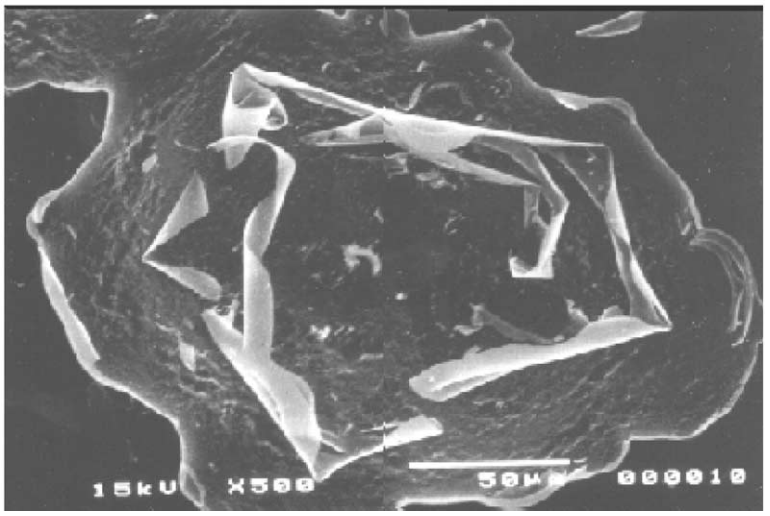

(a)

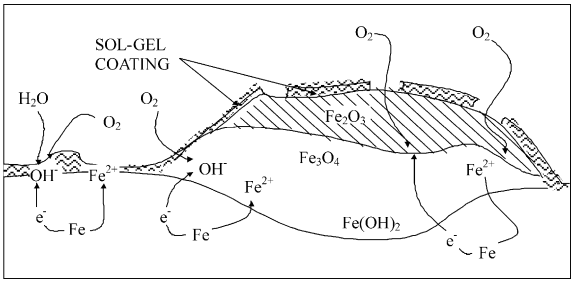

(b)

Fig. 7. (a) SEM image of delamination of 10% MPS sol–gel coating on a stainless steel substrate and (b) a schematic of the delamination mechanism associated with corrosion pitting after polarization analysis.

which was also found at the interface between sol–gel coatings and polyester substrates [18]. In addition, it is anticipated that the incorporation of non-bonding organic components into the sol–gel coatings would result in decreased adhesion between the coating and the substrate as reported in the literature [21]. However, no appreciable influence of the organic component on the adhesion and corrosion protection was observed. It is probable that the organic components were less preferentially resided at the interface, but no experiments have been conducted to verify this hypothesis.

Some preliminary tests showed that the organic–inorganic hybrid coatings possess good biocompatibility. Specifically, no cell lysis or intracytoplasmic granules were noted, which indicated that the organic–inorganic hybrid coatings are non-cytotoxic. Furthermore, the percent of cell lysis was determined to be 0.00% (below the detection limit), and thus the sol–gel coatings are considered to be non-hemolytic. Although the above results are preliminary and further testing is required, the biocompatibility test results are in good agreement with the literature that SiO_2 is a biocompatible material [28,29]. It is noted that the above biocompatibility tests were done on the hybrid coatings consisting of the organic component, or the methacryloxypropyl group, up to 20 mol% MPS. The SiO_2–MPS hybrid coatings are promising candidates for biocompatible applications.

4. Conclusions

Silica-based hybrid coatings, prepared by a two-step acid catalyst sol–gel process, were found uniform, defect-free and relatively dense. Hybrid coatings on stainless steel substrates demonstrated enhanced corrosion protection by forming a physical barrier, which effectively separated the anode from the cathode electrically. It was found that the corrosion protection could be further enhanced with an increased coating thickness. SEM study suggested that interface corrosion is the likely mechanism of breakdown of the sol–gel coatings. The hybrid coatings also demonstrated excellent adhesion and flexibility, which could be attributed to the formation of chemical bonding at the interface and the incorporation of organic components, respectively. In addition, preliminary experiments suggest that the hybrid coatings might have good biocompatibility for bio-medical applications.

Acknowledgements

The authors would like to acknowledge the partial financial support from Boston Scientific and the technical support from Dave Rice and Sam Salamone. S.J.L. would like to acknowledge the NSF-IGERT fellowship and Y.W. the nanotechnology fellowship from the Center for Nanotechnology at the University of Washington.

References

[1] D.A. Jones, Principles and Prevention of Corrosion, 2nd Ed., Prentice-Hall, New Jersey, 1996.
[2] L.L Shreir, R.A. Jarman, G.T. Burstein (Eds.), Corrosion, 3rd Ed., Butterworth-Heinemann, Oxford, 1994.
[3] R. Buchheit, J. Electrochem. Soc. 142 (1994) 3994.
[4] G. Grundmeier, W. Schmidt, M. Stratmann, Electrochim. Acta 45 (2000) 2515.
[5] R. Haneda, K. Aramaki, J. Electrochem. Soc. 145 (1998) 2786.
[6] W. Lu, R.L. Elsenbaumer, T. Chen, V.G. Kulkarni, Mater. Res. Soc. Symp. Proc. 488 (1998) 653.
[7] R. Haneda, K. Aramaki, J. Electrochem. Soc. 145 (1998) 1856.
[8] M. Itoh, H. Nishihara, K. Aramaki, J. Electrochem. Soc. 142 (1995) 3696.
[9] M. Guglielmi, J. Sol–Gel Sci. Technol. 1 (1994) 177.
[10] D.C.L. Vasconcelos, J.N. Carvalho, M. Mantel, W.L. Vasconcelos, J. Non-Cryst. Solids 273 (2000) 135.
[11] M. Simoes, O.B.G. Assis, L.A. Avaca, J. Non-Cryst. Solids 273 (2000) 159.
[12] M. Atik, S.H. Messaddeq, F.P. Luna, M.A. Aegerter, J. Mater. Sci. Lett. 15 (1996) 2051.
[13] P. Neto, M. Atik, L.A. Avaca, M.A. Aegerter, J. Sol–Gel Sci. Technol. 2 (1994) 529.
[14] C.J. Brinker, G.W. Scherer, Sol–Gel Science: The Physics and Chemistry of Sol–Gel Processing, Academic Press, San Diego, 1990.
[15] A.C. Pierre, Introduction to Sol–Gel Processing, Kluwer, Boston, MA, 1998.
[16] L.F. Francis, Mater. Manuf. Process. 12 (1997) 963.
[17] X.H. Han, G.Z. Cao, T. Pratum, D.T. Schwartz, B. Lutz, J. Mater. Sci. 36 (2001) 985.
[18] C.M. Chan, G.Z. Cao, H. Fong, M. Sarikaya, T. Robinson, L. Nelson, J. Mater. Res. 15 (2000) 148.
[19] J. Wen, G.L. Wilkes, J. Inorg. Organometall. Polym. 5 (1995) 343.
[20] J.S. Park, J.D. Mackenzie, J. Am. Ceram. Soc. 78 (1995) 2669.
[21] S.H. Messaddeq, S.H. Pulcinelli, C.V. Santilli, A.C. Guastaldi, Y. Messaddeq, J. Non-Cryst. Solids 247 (1999) 164.
[22] M. Atik, F.P. Luna, S.H. Messaddeq, M.A. Aegerter, J. Sol–Gel Sci. Technol. 8 (1997) 517.
[23] E.P. Plueddemann, Silane Coupling Agents, Plenum, New York, 1982.
[24] G.Z. Cao, Y.F. Lu, L. Delattre, C.J. Brinker, G.P. López, Adv. Mater. 8 (1996) 588.
[25] Y. Massiani, P. Gravier, J.P. Crousier, L. Fedrizzi, P.L. Bonora, 1st Ed., in: J.M. Costa, A.D. Mercer (Eds.), Progress in the Understanding and Prevention of Corrosion, Institute of Materials, London, 1993, p. 179.
[26] C.J. Brinker, A.J. Hurd, P.R. Schunk, G.C. Frye, C.S. Ashley, J. Non-Cryst. Solids 147&148 (1992) 424.
[27] Y.F. Lu, G.Z. Cao, R.P. Kale, S. Prabakar, G.P. López, C.J. Brinker, Chem. Mater. 11 (1999) 1223.
[28] L.L. Hench, Sol–Gel Silica: Properties, Processing and Technology Transfer, Noyes, Westwood, NJ, 1998.
[29] R.K. Iler, The Chemistry of Silica: Solubility, Polymerization, Colloid and Surface Properties, and Biochemistry, Wiley, New York, 1979.